Crystallographic analysis of AcrB

Klaas M. Pos[a,*], André Schiefner[b], Markus A. Seeger[a], Kay Diederichs[b]

[a]*Institut für Mikrobiologie, D-Biol, ETH Zürich, Schmelzbergstr. 7, CH-8092 Zürich, Switzerland*
[b]*Fachbereich Biologie, Universität Konstanz, Universitätsstr. 10, M656, D-78457 Konstanz, Germany*

Abstract A His-tagged derivative of the multidrug efflux pump AcrB could be crystallized in three different space groups (R3, R32 and P321). Experimental MAD-phasing maps from R32 AcrB$_{His}$ crystals were obtained to a resolution of 3.5 Å. Datasets of native and substrate soaked AcrB$_{His}$ crystals were collected at the Swiss Light Source X06SA beamline up to a resolution of 2.7 Å and refinement of these data provided good quality electron density maps, which allowed us to complement the published AcrB structure (PDB code 1iwg). Introduction of amino acids 860–865 and 868 lacking in the 1iwg structure and deletion of a highly disordered region (amino acids 669–678) improved R_{free} and average B factors in the 2.7 Å model. We could not identify significant densities indicating specific antibiotic binding sites in the AcrB R32 space group datasets under the soaking conditions tested.
© 2003 Published by Elsevier B.V. on behalf of the Federation of European Biochemical Societies.

1. Introduction

Bacteria have evolved three general mechanisms of resistance towards antibiotics: (i) resistance by target modification; (ii) resistance by antibiotic modification; and (iii) resistance through the action of antibiotic efflux pumps. Membrane protein pumps responsible for the latter type of resistance can be classified as (i) ABC-type antibiotic resistance pumps, which utilize the free energy of adenosine triphosphate (ATP) hydrolysis to energize the efflux of toxic compounds over the membrane or (ii) secondary antibiotic efflux pumps which use the electrochemical gradient of ions across the membrane in an antiport modus to energize efflux processes.

Secondary antibiotic/multiple drug resistance transporters can be divided into four families [1,2]: (i) major facilitator superfamily (MFS); (ii) small multidrug resistance family (SMR); (iii) multidrug and toxic compound extrusion family (MATE); and (iv) resistance nodulation cell division superfamily (RND, TC# 2.A.6). Members of the RND superfamily involved in the transport of antibiotics belong to the family of the (largely Gram-negative bacterial) hydrophobe/amphiphile efflux-1 (HAE1) family (TC# 2.A.6.2). The proton motive force-driven RND/HAE1 drug/H$^+$ antiporters usually function within a tripartite system including an outer membrane channel (outer membrane factor family (OMF, TC# 1.B.17)) and a member of the membrane fusion protein family (MFP, TC# 8.A.1) (Fig. 1). The drug efflux is believed to occur via the initial binding of the drug to the RND component and subsequent transport through the OMF. The role of the MFP is still puzzling, although it has been shown that it is absolutely essential for the function of the whole pump [3–5]. Besides the well-studied RND–MFP–OMF systems in *Pseudomonas aeruginosa* (e.g. MexAB-OprM and MexCD-OprJ) [6], the AcrAB–TolC tripartite system is currently the most studied due to the structural information on the AcrB and TolC components [7–9]. The substrate specificity of the AcrAB–TolC system is rather broad: anionic, cationic and zwitterionic as well as neutral compounds are transported, including fluoroquinolones, macrolides and phenylpropanoids. Most of the substrates are hydrophobic and can traverse the inner membrane. A notable exception are the β-lactams transported by the system [10]. TolC has been structurally characterized to a resolution of 2.1 Å by crystallographic means [9]. Apart from the membrane-embedded regions (about 4 nm thickness), a TolC trimer has a 10 nm periplasmic barrel domain composed of 12 α-helices, which form a long conduit through which the drugs might be transported. The crystallization and structural analysis of AcrB have been described recently [8,11]. Like TolC, AcrB forms a homotrimer, which is believed to be its functional unit. Each AcrB monomer contains 12 membrane spanning α-helices and a large periplasmic domain (Fig. 2A). The transmembrane α-helices in the AcrB trimer are organized in a way that these encircle a 35 Å wide cavity, which is believed to be filled with phospholipids in vivo (Fig. 2B). Within each monomer, transmembrane helices 4 and 10, encircled by the other transmembrane helices of the monomer, harbor the residues Lys940 (helix 10) and Asp407 and 408 (helix 4), which are postulated to be important for the H$^+$ translocation (Fig. 2B and [8]). The periplasmic domain can be divided into two major parts: the TolC docking domain and the pore domain. The TolC docking domain exhibits a funnel-like structure narrowing to the central pore located in the pore domain. The internal diameter on the top of the funnel is about the same as the diameter of the TolC periplasmic conduit. The central pore structure consists of three α-helices, one donated by each AcrB monomer (Fig. 2C). Another remarkable feature is a long loop protruding from one monomer through the neighboring monomer. These loops appear to make the main and almost only interaction between the monomers. At the prox-

*Corresponding author. Fax: (41)-1-632 5523.
E-mail address:* pos@micro.biol.ethz.ch (K.M. Pos).

Abbreviations: CHM, cyclohexyl-*n*-hexyl-β-D-maltoside; SeMet, selenomethionine
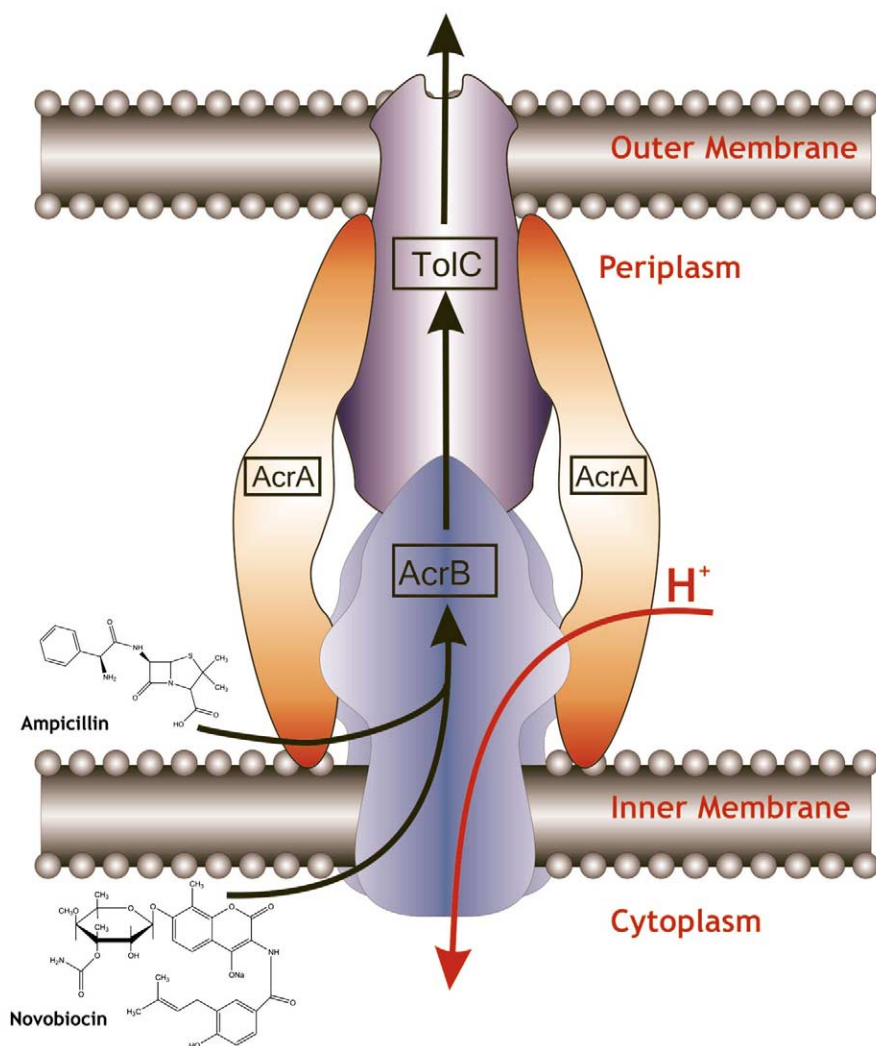
Fig. 1. Hypothetical structure of tripartite efflux pumps in Gram-negative bacteria, e.g. the AcrAB–TolC efflux pump from *E. coli* (adapted from Nikaido and Zgurskaya [10]).

imal end of the central pore, the structure opens up to a central cavity, leading to the cavity in the transmembrane part. Moreover, three entrances or vestibules reaching towards the central cavity are located just above the membrane plane. From the AcrB native structure a drug transport model has been postulated [8,12] which involves the transport of membrane permeable drugs from the inner leaflet of the cytoplasmic membrane through a groove formed by transmembrane helices 8 and 9 towards the central cavity. β-Lactam antibiotics are believed to enter the central cavity via the vestibules. Once in the central cavity, the substrates are believed to be transported into the external medium through the central pore (which has to open first), through the funnel part of the AcrB periplasmic domain and finally through TolC. Currently, the elucidation of the molecular mechanism(s) of transport of the wide variety of substrates is a major challenge. The substrate binding and specificity has already been addressed by structural and functional studies. It has been shown that the periplasmic part of the RND component is responsible for the substrate specificity of the whole tripartite system. This has been demonstrated for AcrB, MexB, MexD, and MexY [13–15]. Additionally, structural analysis of binding of antibiotics to AcrB (based on 3.5–3.8 Å data) has been

reported recently [7]. Binding of four AcrB substrates, rhodamine G6, ethidium, dequalinium and ciprofloxacin is observed in the central cavity. For all substrates except ciprofloxacin, Phe386 (helix 3) was one of the main hydrophobic contacts, in fact in the case of ethidium it seemed to be the only one. For dequalinium, only the top quinolinium moiety was close to the charged residues Asp99 and 101 but the bottom quinolinium moiety was close to only Phe386. For ciprofloxacin, Phe458 and 459 (helix 5) were the main ligands. Binding of three substrate molecules per trimer was observed as enforced by the three-fold symmetry of the R32 space group. Another observation was an 1° outward tilting of the periplasmic domain, postulated to be induced by the substrate binding [7].

We report here on the crystallographic analysis of diffraction data obtained (up to 2.7 Å) with crystals from native AcrB$_{His}$, a selenomethionine (SeMet) substituted derivative and substrate soaked derivatives of AcrB$_{His}$.

2. Materials and methods

2.1. Crystal optimization and SeMet substitution

Expression of *acrB$_{His}$*, preparation of membranes, purification and initial crystallization of AcrB$_{His}$ are described in Pos and Diederichs [11]. To obtain SeMet substituted AcrB, *Escherichia coli* C43(DE3)/
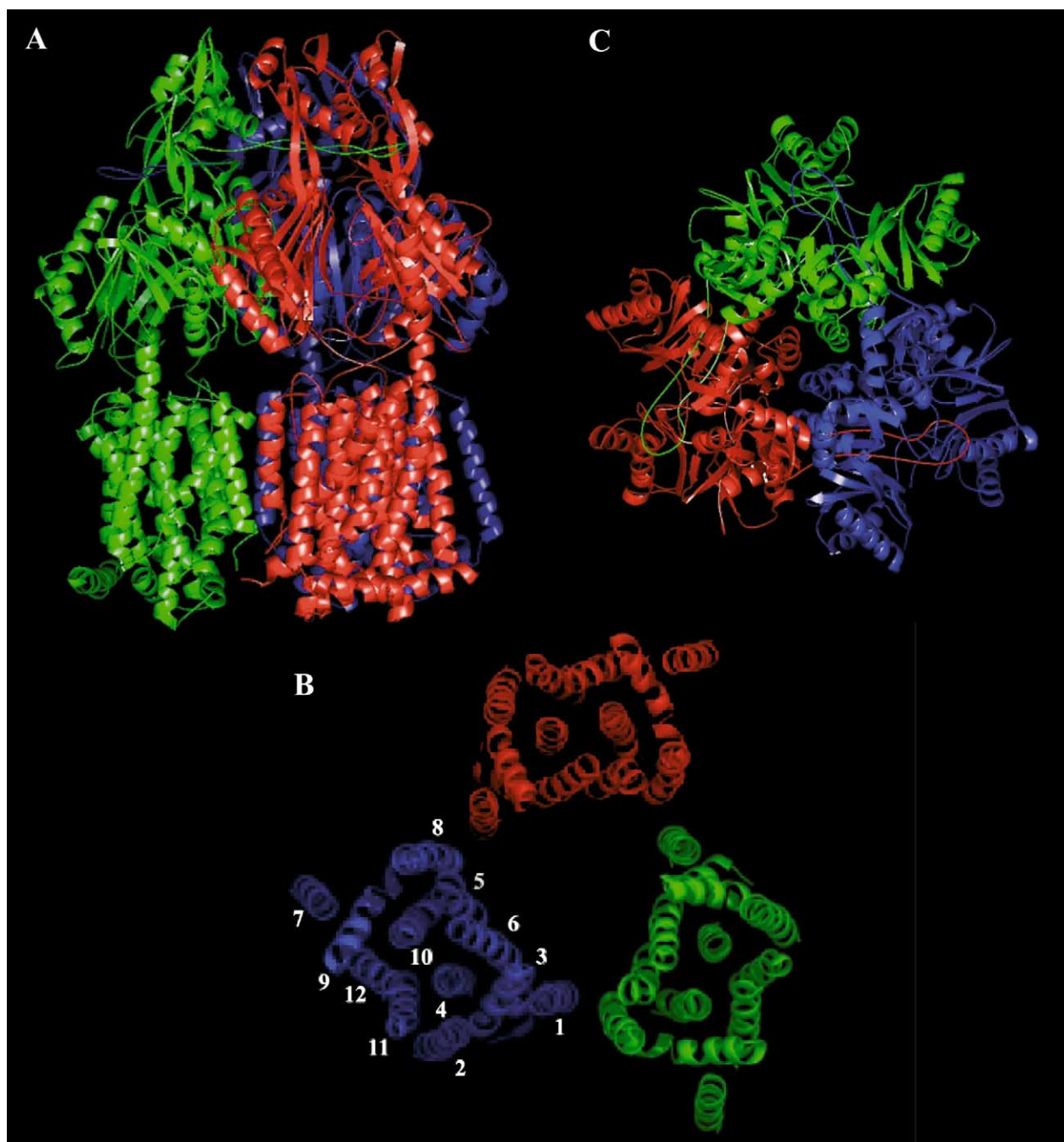
Fig. 2. A: Backbone ribbon diagram side view of AcrB trimer. B: Topology of the transmembrane helices top view along the crystallographic three-fold axis. The three monomers enclose a 30–35 Å wide cavity. C: Backbone periplasmic top view along the crystallographic three-fold axis. The long loops protruding from one monomer into the next provide the main interaction within the AcrB trimer. The protomers are individually colored. Figures are Pymol (www.pymol.org) drawings based on the coordinates deposited in the PDB databank entry 1iwg [8].

pET24acrB$_{His}$ was grown in methionine deprived minimal media including SeMet. Yields were 6 mg of SeMet substituted AcrB$_{His}$ from 1 l of minimal media culture. SeMet crystals ($200 \times 200 \times 100$ μm^3) were grown using 0.1 M Na-HEPES, pH 7.5, 10–60 mM NaCl and 8% (w/v) PEG 4000 as precipitant and protein at 39 mg/ml in a hanging drop (1:1 dilution) experimental setup over a 0.5 ml precipitant solution in the reservoir. Crystals which belong to the space group R32 were frozen in liquid ethane using glycerol as cryoprotectant. AcrB$_{His}$ R3 crystals were obtained using 17 mg/ml protein diluted 1:1 in 0.1 M Na-HEPES, pH 7.5, 50 mM NaCl, 5% (v/v) glycerol and 5% (w/v) PEG 4000 as precipitant in a hanging drop experimental setup over a 0.5 ml precipitant solution in the reservoir. P321 crystals (about $100 \times 100 \times 10$ μm^3) were obtained using 70 mM

Na-citrate, pH 4.6, 8% (v/v) glycerol and 16% (v/v) PEG 400 as precipitant (1:1 dilution, hanging drop). For freezing these crystals, solid glucose was added to the droplet containing the crystal and allowed to saturate the drop in a stepwise manner. Large single native AcrB$_{His}$ (R32) crystals with dimensions up to $1000 \times 800 \times 400$ μm^3 were obtained by adding isopropyl-β-D-thiogalactopyranoside, n-decanoylsucrose, n-nonyl-β-D-thiomaltoside or n-octyl-β-D-thiomaltoside (at 1% (w/v), 2.5, 3.2 and 9 mM final concentration, respectively). AcrB$_{His}$ was used at 16.8 mg/ml. Crystals were transferred in 11 steps to 0.1 M Na-HEPES, pH 7.5, 5% (w/v) PEG 4000, 0.1 M NaCl and 0.05% (w/v) cyclohexyl-n-hexyl-β-D-maltoside (CHM) solutions containing 2–30% (v/v) glycerol in 5–10 min intervals. After the final soaking step at 30% (v/v) glycerol, the crystals were directly frozen
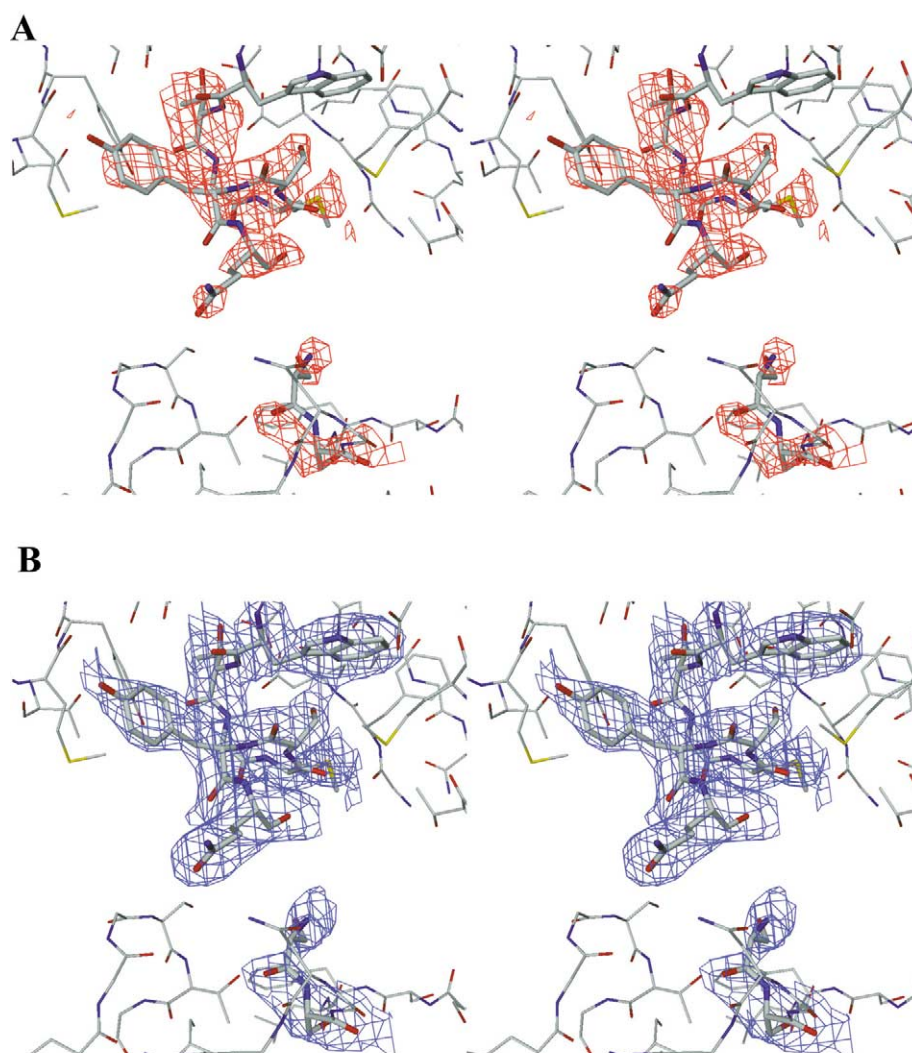
Fig. 3. Stereo view displaying the region 860–868 with (A) the F_o-F_c map at 2.7 Å contoured at 3σ in red and (B) $2F_o-F_c$ electron density map at 2.7 Å contoured at 1σ in blue. Shown in bold sticks from top to bottom are the residues Trp859 and the amended residues Thr860, Gly861, Met862, Ser863, Tyr864, Gln865, Leu868 and Ser869.

into liquid propane or ethane and stored in liquid nitrogen. In soaking experiments, crystals were treated using the same procedure in the presence of 0.5–5 mM bile salt or antibiotic.

2.2. X-ray diffraction dataset analysis and refinement procedure

Datasets from native crystals and heavy atom derivatives were collected at the DESY, Hamburg, Germany, EMBL beamlines BW7A, BW7B and X11. Native and substrate co-crystals as well as the MAD data were measured either at beamline X06SA of the Swiss Light Source (Paul Scherrer Institut, Villigen, Switzerland) or at beamline ID29 of the ESRF (Grenoble, France). Data reduction was done with the XDS Software package [16]. The SeMet substructure of the SeMet derivative crystals was solved with SHELXD [17]. A total of 35 selenium sites out of 42 theoretically possible sites could be detected. Further refinement of the heavy atom positions was carried out with the program SHARP [18]. Solvent flattening with RESOLVE [19,20] resulted in interpretable maps at a resolution of 3.5 Å. The structures in the other space groups were solved by molecular replacement using MOLREP [21]. As search models 1iwg and a modified version of 1iwg (model2, see Section 3) were used. All structures were refined with the program REFMAC5 [22] starting with 20 cycles of rigid body refinement with four rigid domains consisting of residues (i) 1–30 and 334–530, (ii) 31–333, (iii) 561–859 and (iv) 531–560 and 860–1031, followed by 20 cycles of restrained refinement. Model

building was done using the program 'O' [23]. Fig. 2 was created using Pymol (www.pymol.org) and Figs. 3 and 4 were created using DINO (www.dino3d.org).

3. Results and discussion

3.1. Diffraction quality of AcrB$_{His}$ crystals

The first crystals of AcrB$_{His}$ in space group R32 were obtained in a screening procedure using the MembFac screen of Hampton (solution 30) and were rather sensitive to radiation damage [11]. The initial cryoprotection procedures led to cracking of larger crystals while freezing them in liquid nitrogen. These problems could be overcome by the optimization of the crystallization conditions and freezing protocol. Crystals grown in the presence of n-nonyl-β-D-thiomaltoside and n-octyl-β-D-thiomaltoside were transferred into cryoprotection solutions containing 1 mM erythromycin or novobiocin, respectively, in the case of substrate binding studies. After the final soaking step, the crystals were directly frozen in liquid propane or ethane and stored in liquid nitrogen. This proce-
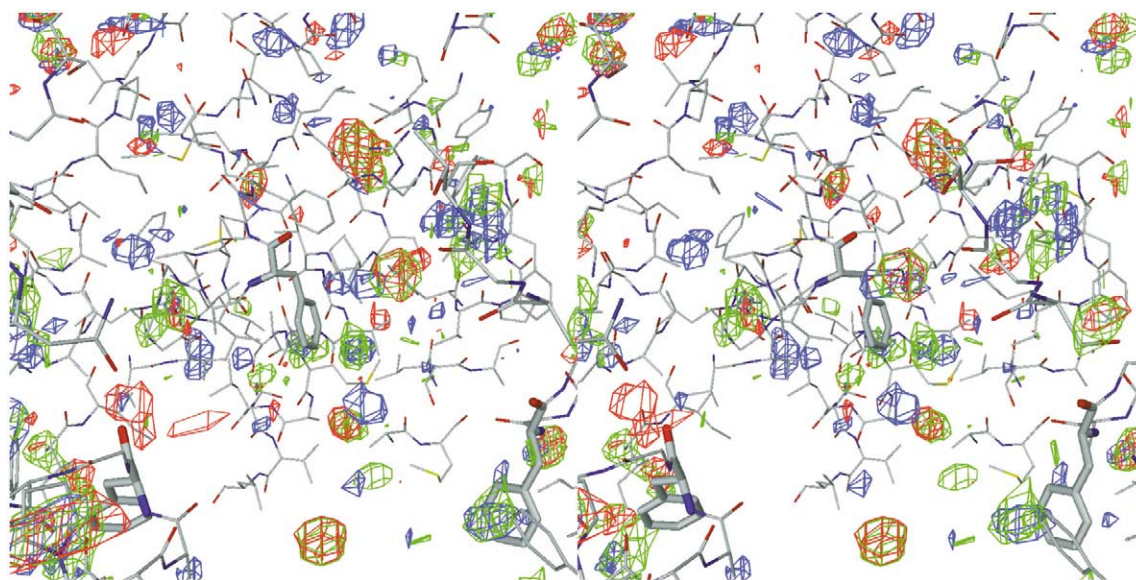
Fig. 4. Trimer central cavity region near Phe386 (bold stick): Stereo view of F_o-F_c electron density maps at 2.9 Å contoured at 3σ: blue: m209 (native), green: m227 (erythromycin soaked), red: m228 (novobiocin soaked).

dure improved the diffraction of the crystals to a resolution of 2.7 and 2.8 Å, for the native and substrate soaked crystals, respectively.

AcrB could be crystallized in two other space groups, R3 and P321. R3 crystals were obtained using the same crystallization conditions as described for R32 crystals, but with addition of 5% (v/v) glycerol in the mother liquor and 2.5% (v/v) glycerol in the initial protein droplet condition. These crystals ($350\times350\times300$ μm^3) diffracted to 3.0 Å resolution. P321 crystals (about $100\times100\times10$ μm^3) were obtained using 70 mM Na-citrate, pH 4.6, 8% glycerol and 16% (v/v) PEG 400 as precipitant. These crystals were frozen using glucose as cryoprotectant. One dataset has been collected to a resolution of 3.5 Å.

3.2. Structure solution and refinement

In order to obtain phase information, R32 crystals were soaked with various heavy atom compounds. Despite good datasets (to 3.0 Å resolution), phases could not be determined due to severe non-isomorphism. Especially the c-axis of the crystal unit cell varied drastically (between 490 and 520 Å), which made direct comparison of the datasets impossible. We therefore produced crystals of SeMet substituted AcrB$_{His}$ and

collected MAD data (Table 1). After determining phases using the programs SHELXD, SHARP and RESOLVE, interpretable electron density maps were obtained at 3.5 Å resolution. During the process of model building, Murakami et al. [8] published a structure of AcrB based on 3.5 Å diffraction data. Their model (PDB database entry 1iwg) was used in the initial refinement procedures with our diffraction data.

The refinement statistics listed in Table 2 clearly demonstrate that our experimental data from native and substrate soaked crystals produced models of AcrB with high R_{free} values after rigid body and restrained refinement. The highest R_{free} values were observed with data from a R32 crystal soaked with taurocholate (m215, 3.1 Å, $R_{free}=42.6\%$) and with the native R3 crystal dataset (m1, 3.0 Å, $R_{free}=41.8\%$). The best R_{free} values were obtained with the native crystal dataset m237 (3.0 Å, $R_{free}=36.2\%$) and the data from the novobiocin soaked crystal m228 (2.8 Å, $R_{free}=35.8\%$). In comparison, the 1iwg structure published by Murakami et al. [8] yielded an R_{free} value of 35.5% (at 3.5 Å) and the unliganded structure 1oy6 published by Yu et al. [7] showed an R_{free} of 33.0% at 3.7 Å. The average B factors from the refined structures based on 1iwg are in almost all cases above 100 Å^2, with the notable exception of the m1 3.0 Å dataset in

Table 1
Data collection and crystallographic analysis

	Peak	SeMet inflection	Remote	Native	Native	Native
Space group	R32			R32	R3	P321
Cell axes (Å)	$a=b=146.2$; $c=520.0$			$a=b=143.7$; $c=513.9$	$a=b=145.4$; $c=519.2$	$a=b=133.1$; $c=192.2$
Wavelength (Å)	0.9792	0.9791	0.9756	0.9774	0.9796	0.9790
Resolution (Å)	3.5	3.5	3.5	2.65	3.2	3.5
Observations	323 212	438 015	289 466	539 666	127 510	313 867
Unique reflections	52 275	52 273	50 259	59 390	66 801	25 414
Completeness (%)	99.9	99.9	96.1	99.2	99.0	99.9
$I/\sigma(I)$	7.0	7.4	9.4	15.5	5.4	10.3
R_{merge} (%)	30.1	32.4	23.3	8.2	9.9	19.8
R_{mrgd-F}[a] (%)	24.1	23	19.8	7.3	21.5	16.8
Anomalous phasing power (acentric)	1.6	0.9	1.5			
Overall figure of merit:		0.47				

[a] R_{mrgd-F} is a measure for the quality of the reduced amplitudes [24].

Table 2
Refinement statistics after rigid body and restrained refinement

Crystal name	Resolution range (Å)	R factor (%)	R_{free} (%)	rms bond length (Å deviation)	rms bond angles (degrees deviation)	Average B factor (Å^2)
M1 (R3 native)						
1iwg	19.7–3.0	36.2	41.8	0.013	1.48	61.6
model2	19.7–3.0	36.0	41.1	0.013	1.42	61.6
M209 (native)						
1iwg	19.5–2.65	34.1	37.2	0.009	1.19	100.7
model2	182.5–2.65	34.5	36.4	0.010	1.27	67.5
M210 (native)						
1iwg	19.8–3.0	37.0	39.0	0.011	1.32	110.0
model2	19.8–3.0	35.6	37.0	0.013	1.40	74.7
M237 (native)						
1iwg	46.6–3.0	33.5	36.2	0.011	1.32	102.8
model2	46.6–3.0	32.9	35.0	0.011	1.32	76.3
M238 (native+IPTG)						
1iwg	46.6–2.9	37.3	39.8	0.011	1.32	118.7
model2	46.6–2.9	35.6	38.7	0.012	1.37	91.5
M198 (Hoechst 33342)						
1iwg	47.7–2.9	37.6	39.7	0.010	1.28	109.0
model2	47.7–2.9	34.7	38.4	0.011	1.29	85.4
M215 (taurocholate)						
1iwg	47.1–3.1	40.1	42.6	0.011	1.32	112.2
model2	47.1–3.1	37.6	39.4	0.013	1.41	90.9
M216 (taurocholate)						
1iwg	46.6–3.0	35.5	39.3	0.011	1.32	114.7
model2	46.6–3.0	33.5	37.7	0.011	1.34	88.4
M222 (lomefloxacin)						
1iwg	47.7–3.1	40.0	41.4	0.013	1.41	112.6
model2	47.7–3.1	38.8	40.3	0.015	1.50	95.1
M227 (erythromycin)						
1iwg	46.6–2.9	34.0	39.9	0.011	1.28	98.1
model2	46.6–2.9	34.3	40.1	0.011	1.26	73.4
M228 (novobiocin)						
1iwg	47.7–2.8	33.1	35.8	0.010	1.27	105.6
model2	47.7–2.8	33.9	36.8	0.010	1.26	81.6
M240 (erythromycin)						
1iwg	46.1–3.1	36.1	40.2	0.011	1.36	124.7
model2	46.1–3.1	33.4	37.8	0.013	1.42	104.1
M241 (erythromycin)						
1iwg	47.0–3.0	33.8	37.7	0.012	1.42	109.3
model2	47.1–3.0	34.8	37.1	0.013	1.43	92.9

R3 (61.6 Å^2). High average B factors were also found for the structures 1iwg [8] and 1oye [7].

Due to disorder, the 1iwg AcrB model lacks regions 1–6, 499–512, 860–868 and 1037–1049 [8]. Inspection of our F_o-F_c and $2F_o-F_c$ maps obtained with datasets m1, m209, m227 and m228 (Table 2) revealed the presence of interpretable density in the region of residues 860–868 (Fig. 3a and b). We amended the model in this region by implementing amino acid residues 860–865 and 868. Furthermore, we corrected the side chain location of Glu112 (pore region) and His596 and deleted amino acids 669–678 due to poor electron density. The modified model (designated model2) resulted in slightly better R_{free} factors in the refinement cycle compared to the same refinement done with 1iwg (Table 2). The best R_{free} factor was obtained with the datasets from native R32 crystals using this modified model. Refinement against data from crystal m237 yielded an R factor of 32.9% and R_{free} of 35.0%. The electron density in the omitted region 669–678 after refinement with model2 is difficult to interpret and requires further analysis before an alternate chain progression can be determined. Remarkably, the B factors dropped approximately 10–30% compared to the refined 1iwg structure (Table 2).

3.3. Substrate binding studies

We have tested several compounds (erythromycin, novobiocin, taurocholate, taurodeoxycholate, lomefloxacin, ciprofloxacin, deoxycholate, chloramphenicol and Hoechst 33342) for binding to AcrB$_{His}$ by crystal soaking experiments and occasionally by co-crystallization. All data obtained from compound soaked crystals resulted in higher R factors, with the exception of m228 (novobiocin soak, R_{free} = 35.8% with 1iwg and 36.8% with model2). Very high R factors were obtained with the lomefloxacin and erythromycin soaked crystal datasets m222 and m227 (= 40%). In comparison, Yu et al. [7] reported almost equal R_{free} factors for the unliganded and liganded structures (32–34%) at 3.5–3.8 Å. Our experimental setup differs from that described in Yu et al. [7] by (i) the presence of a His-tag at the C-terminus of the protein, (ii) a higher pH of the soaking buffer (7.5 versus 5.6 and 6.6) and (iii) the use of CHM (0.05%) rather than dodecyl-β-D-maltoside (DDM) (0.1%) as detergent. Furthermore, in the determination of drug binding sites, Yu et al. [7] used electron density omit maps directly after data scaling and molecular replacement, before doing any refinement. We calculated the F_o-F_c and $2F_o-F_c$ maps (Fig. 4) after molecular replacement

and refinement (rigid body and restrained refinement with REFMAC5). Inspection of $F_o - F_c$ difference maps using our substrate soaked crystal datasets did not reveal any significant positive density features different from the ones observed with the native datasets (Fig. 4). The $2F_o - F_c$ maps of m209 (native), m227 (erythromycin soaked crystal) and m228 (novobiocin soaked crystal) at 2.7–2.8 Å all showed similar density features (not shown). Despite the good resolution of the density maps (2.8 Å), we were not able to identify difference density features that could be attributed to bound ligands. A possible reason for this is the low quality of the phases derived from a high R factor model. We expect that a future improvement of the AcrB model (with lower R_{free}) might lead to the unambiguous identification of substrate binding sites, allowing a deeper understanding of the functional aspects of AcrB.

References

[1] Busch, W. and Saier Jr., M.H. (2002) Crit. Rev. Biochem. Mol. Biol. 37, 287–337.

[2] Busch, W. and Saier Jr., M.H. (2003) Methods Mol. Biol. 227, 21–36.

[3] Ma, D., Cook, D.N., Alberti, M., Pon, N.G., Nikaido, H. and Hearst, J.E. (1993) J. Bacteriol. 175, 6299–6313.

[4] Zgurskaya, H.I. and Nikaido, H. (1999) Proc. Natl. Acad. Sci. USA 96, 7190–7195.

[5] Zgurskaya, H.I. and Nikaido, H. (1999) J. Mol. Biol. 285, 409–420.

[6] Poole, K. (2001) J. Mol. Microbiol. Biotechnol. 3, 255–264.

[7] Yu, E.W., McDermott, G., Zgurskaya, H.I., Nikaido, H. and Koshland Jr., D.E. (2003) Science 300, 976–980.

[8] Murakami, S., Nakashima, R., Yamashita, E. and Yamaguchi, A. (2002) Nature 419, 587–593.

[9] Koronakis, V., Sharff, A., Koronakis, E., Luisi, B. and Hughes, C. (2000) Nature 405, 914–919.

[10] Nikaido, H. and Zgurskaya, H.I. (2001) J. Mol. Microbiol. Biotechnol. 3, 215–218.

[11] Pos, K.M. and Diederichs, K. (2002) Acta Crystallogr. D Biol. Crystallogr. 58, 1865–1867.

[12] Murakami, S. and Yamaguchi, A. (2003) Curr. Opin. Struct. Biol. 13, 443–452.

[13] Tikhonova, E.B., Wang, Q. and Zgurskaya, H.I. (2002) J. Bacteriol. 184, 6499–6507.

[14] Eda, S., Maseda, H. and Nakae, T. (2003) J. Biol. Chem. 278, 2085–2088.

[15] Elkins, C.A. and Nikaido, H. (2002) J. Bacteriol. 184, 6490–6498.

[16] Kabsch, W. (1993) J. Appl. Cryst. 26, 795–800.

[17] Schneider, T.R. and Sheldrick, G.M. (2002) Acta Crystallogr. D Biol. Crystallogr. 58, 1772–1779.

[18] Bricogne, G., Vonrhein, C., Flensburg, C., Schiltz, M. and Paciorek, W. (2003) Acta Crystallogr. D Biol. Crystallogr. 59, 2023–2030.

[19] Terwilliger, T.C. (2000) Acta Crystallogr. D Biol. Crystallogr. 56, 965–972.

[20] Terwilliger, T.C. (1999) Acta Crystallogr. D Biol. Crystallogr. 55, 1863–1871.

[21] Vagin, A.A., Teplyakov, A. (1997) J. Appl. Cryst. 30, 1022–1025.

[22] Murshudov, G.N., Vagin, A.A. and Dodson, E.J. (1997) Acta Crystallogr. D Biol. Crystallogr. 53, 240–255.

[23] Jones, T.A., Zou, J.Y., Cowan, S.W. and Kjeldgaard, M. (1991) Acta Crystallogr. A 47, 110–119.

[24] Diederichs, K. and Karplus, P.A. (1997) Nat. Struct. Biol. 4, 269–275.